Journal of Porous Materials (2018) 25:1251–1264
https://doi.org/10.1007/s10934-017-0536-5

Synthesis of Fe_3O_4 modified mesoporous silica hybrid for pH-responsive drug delivery and magnetic hyperthermia applications

Madhappan Santha Moorthy[1] · Subramanian Bharathiraja[1] · Panchanathan Manivasagan[1] · Yunok Oh[1] · Thi Tuong Vy Phan[2] · Sudip Mondal[1] · Hyehyun Kim[2] · Kang Dae Lee[3] · Junghwan Oh[1,2]

Published online: 15 November 2017

Abstract
The chemotherapy combined with thermotherapy is greatly considered in clinical applications for cancer treatment. The fabrication of nanomaterials with multifunctionality is an attractive approach to be utilized in cancer therapy. In this work, we report the synthesis of dopamine-urea organosilane (DPU) integrated mesoporous silica material in which the magnetic Fe_3O_4 nanoparticles were grown onto the outer surface of the mesoporous silica nanoparticles via Fe_3O_4-dopamine complexation method. The mesoporous structural characterization results revealed that the synthesized Fe_3O_4@DPU@MSH materials had high surface area (386 m^2/g), large pore size (4.5 nm) and uniform particles in which the magnetic Fe_3O_4 nanoparticles were grown onto the outer surface of the mesopore walls with the particles size about 5–10 nm. Because of the existence of Fe_3O_4 nanoparticles onto the outer surface of the Fe_3O_4@DPU@MSH material, the sample shows superparamagnetic properties and high magnetic hyperthermia ability in the presence of applied magnetic field. Furthermore, owing to the presence of high surface area, the Fe_3O_4@DPU@MSH shows high drug loading capacity, and pH-responsive and temperature-accelerated drug release efficiency. In addition, the MTT assay analysis and the intracellular uptake study results support that the synthesized Fe_3O_4@DPU@MSH material is biocompatible. Therefore, the Fe_3O_4@DPU@MSH material would be a promising material for drug delivery and magnetic hyperthermia applications in cancer therapy.

Keywords Silica materials · Magnetic nanoparticles · Drug delivery · Magnetic hyperthermia · Biocompatibility

1 Introduction

Recent research mainly focusing to design nanomaterials with two or multi-functions together in a single system to improve their efficiency [1]. Specifically, the nanomaterial-based research is gaining great attention due not only to their unique physicochemical properties but also for their excellent practical applications in several fields such as catalysis, sensors, environmental remediation, drug/gene delivery and biomedical applications [2–6]. The ordered mesoporous silica materials are considered to be promising materials owing to their excellent physicochemical properties such as high surface area, uniform pore size and mesopore volume, chemical, mechanical and thermal stability and biocompatibility [7, 8]. The incorporation of organic functional groups with the mesoporous silica materials would expand their utilisation in various fields. However, for the potential applications, organic functional groups modified mesoporous silica hybrid materials show excellent properties as compared to pure inorganic mesoporous silica (MCM-41, SBA-15) materials owing to their unique organic functionalities.

Recently, the iron oxide-based magnetic mesoporous silica nanomaterials have attracted immense research interest owing to their non-toxic nature, biodegradability and easy separation by external magnetic field and recyclability [9, 10]. Therefore, much research efforts have been given to fabricate the magnetic nanoparticle-based mesoporous silica materials for various applications [11–15]. The incorporation of magnetic nanoparticles onto the outer surface of the

✉ Junghwan Oh
jungoh@pknu.ac.kr

[1] Marine-Integrated Bionic Research Center, Pukyong National University, Busan 48513, Republic of Korea

[2] Department of Biomedical Engineering and Center for Marine-Integrated Biotechnology (BK21 Plus), Pukyong National University, Busan 48513, Republic of Korea

[3] Department of Otolaryngology-Head and Neck Surgery, Kosin University College of Medicine, Busan 48513, Republic of Korea

mesoporous silica nanoparticles have advantages such as (i) due to the existence of the incorporated magnetic nanoparticles onto the outer surface, the mesopore channels remains unoccupied and it is possible to increase the loading efficiency of the desired guest molecules; (ii) fast accumulation kinetics could be achieved under an external magnetic field [16]. The incorporation of small size magnetic Fe_3O_4 nanoparticles onto the outer silica surfaces by metal–ligand complex coordination interaction approach may be an easy approach to grow magnetic nanoparticles onto the outer surfaces of the mesoporous silica nanoparticles [17]. Owing to the formation of magnetic nanoparticles onto the outer silica surfaces, the inner pore channels of the mesoporous silica materials remain unoccupied and they can access the large amount of payloads. Furthermore, due to the existence of magnetic nanoparticles onto the outer surface of the silica nanoparticles it can enhance the heating efficiency in the presence of applied external magnetic field. Magnetic hyperthermia is a promising technique in cancer thermotherapy because the magnetic nanoparticles can generate heat in the presence of applied external magnetic field [18–21]. As compared to the normal cells, tumour tissues are more sensitive to heat and undergo cell apoptosis under hyperthermia temperature (42–45 °C) conditions [22]. Therefore, much efforts have been given to design the nanotherapeutic system which favours the drug delivery and hyperthermia features together in a single system. The concomitant delivery of therapeutic agents and intracellular local hyperthermic heat into the tumour sites can effectively improve the synergistic effects of cancer therapy [23]. The major advantages of the magnetic mesoporous silica-based drug delivery system is that the nanoparticles can be injected into the body and further concentrated in the required target sites simply by applying external magnetic field. Therefore, such drug carrier systems can effectively deliver the anticancer drugs at target sites without affecting normal cells. The stimuli-responsive nanoparticle-based drug delivery carriers are considered to be an excellent platform for cancer therapy. Because, these nanomaterials are sensitive to the intracellular stimuli (pH, enzyme and redox potential) and/or external stimuli (light, magnetic field and temperature) [24].

Among various stimulus, pH stimuli is considered to be efficient because of the pH gradient between normal cells and tumour tissues in the body. Most of the tumour tissues are in acidic pH (pH < 7.4) as compared to normal healthy tissues (pH 7.4) which favours for the target drug delivery [25]. Similarly, the magnetic field is considered to be an effective stimulus because it can be applied externally at the target tumour sites [26]. Current researchers mainly focusing to design nanomaterials which combine dual- or multi-stimuli such as pH/temperature, pH/magnetic field, enzyme/temperature, pH/magnetic field/redox, enzyme/redox/light, etc. to improve the combined therapeutic efficacy [27]. In the pH/temperature stimuli-responsive drug carrier system, the encapsulated drug molecules are retained into the nanocarrier at physiological pH conditions (pH 7.4) and start to deliver the loaded drugs under acidic pH (pH < 7.0) environments. Furthermore, the temperature stimuli can increase the solubility and enhance the diffusion rate of the drug molecules from the drug carrier system.

However, many reports were represent the fabrication of magnetic-based mesoporous silica nanoparticles. Among, most of the reports were discussed the fabrication of core–shell based magnetic mesoporous silica materials [28–30]. Only few works were reported on the synthesis of magnetic mesoporous silica nanoparticles in which the magnetic particles were incorporated inside the mesopore walls [31].

As compared to the core–shell magnetic mesoporous silica materials, the incorporation of magnetic nanoparticles inside the mesopore walls is considered to be efficient because the materials can provide high magnetic heating efficiency. Furthermore, the integrated DPU units can act as drug binding sites which favors more drug loading and pH-responsive drug release efficiency. Herein, we synthesise a magnetic mesoporous silica hybrid material in which the magnetic iron oxide (Fe_3O_4) nanoparticles were grown onto the outer surface of the mesoporous silica hybrid materials through metal–ligand complex coordination method. Firstly, the mesoporous silica hybrid materials were synthesized by using dopamine-urea organosilane (DPU) precursor along with tetraethyl orthosilicate (TEOS) as silica sources by co-condensation method under basic condition. Secondly, the outer surface of the as-synthesized nanoparticles were modified using DPU precursor. Thirdly, the magnetic iron-oxide Fe_3O_4 nanoparticles were grown onto the outer surface of the as-synthesized silica nanoparticles by introducing ferric chloride solution followed by reduction method. Finally, the occluded surfactant into the mesopore channels were removed by solvent extraction process to obtain magnetic mesoporous silica hybrid (Fe_3O_4@DPU@MSH) materials (Scheme 1). The synthesised Fe_3O_4@DPU@MSH material could be desirable to achieve the pH-responsive controlled drug delivery and magnetic hyperthermia applications together in a single entity (Scheme 2). Magnetic hyperthermia treatment may induce anticancer immunity without adverse side effects to the normal cells and the mesoporous silica hybrid assists high drug loading and controlled release of anticancer agents. By combining the pH-responsive drug delivery with magnetic hyperthermia techniques together in a single system allows not only the accumulation of drug in the desired sites in the body but also the possibility of using hyperthermia technique in cancer therapy. Hence, the synthesised Fe_3O_4@DPU@MSH material is suitable to achieve the synergistic effects such as chemotherapy and thermotherapy treatment in cancer therapy.

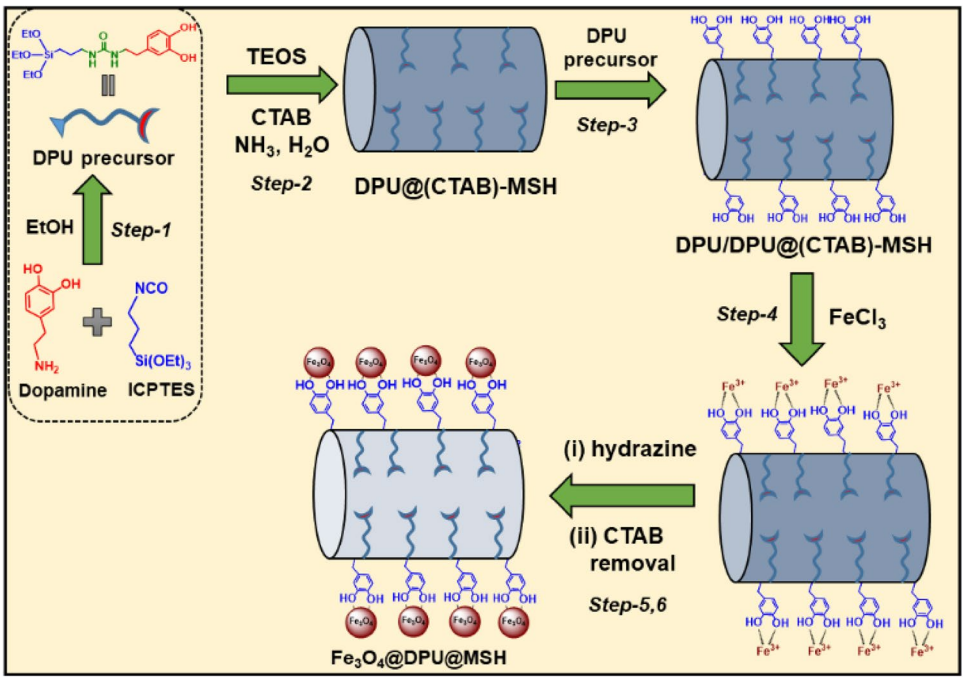

Scheme 1 Schematic representation for the step-wise synthesis and surface fabrication of magnetic Fe_3O_4 nanoparticles onto the Fe_3O_4@DPU@MSH materials

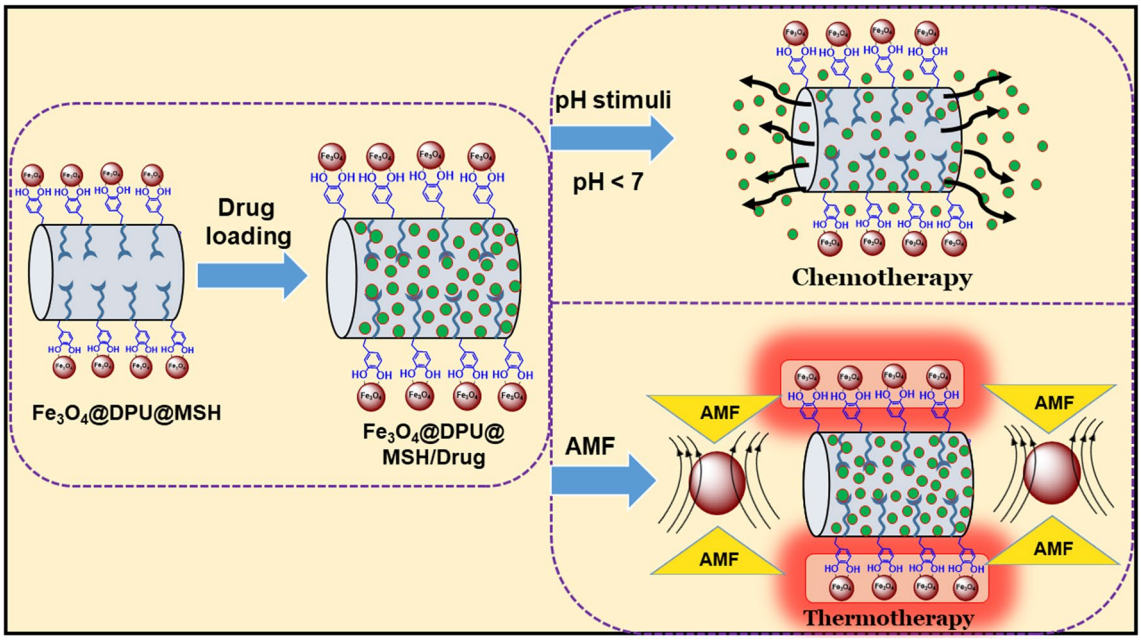

Scheme 2 Schematic representation for the drug loading into the Fe_3O_4@DPU@MSH materials and the pH-responsive drug release, and magnetic hyperthermia applications

2 Experimental

2.1 Materials and reagents

3-(Triethoxysilyl)propyl isocyanate (ICPTES, 95%), tetraethyl orthosilicate (TEOS, 98%), ferric chloride hexahydrate ($FeCl_3 \cdot 6H_2O$), dopamine hydrochloride (98%), hydrazine, ammonium hydroxide (28%), 5-fluorouracil (5-FU) and rhodamine 123 (Rh123) were purchased from Sigma Aldrich (USA) and all the reagents were used as received without further purification.

2.2 Synthesis of dopamine-urea (DPU) precursor

To synthesize dopamine-urea silane precursor, about 0.25 g (1.6 mmol) of dopamine hydrochloride was dissolved in 60 mL of anhydrous ethanol. To this, 0.4 g (1.6 mmol) of ICPTES was added with vigorous stirring under inert condition in the presence of trimethylamine base. The reaction mixture was stirred at 70 °C for 24 h. In this reaction, the isocyanate groups can also possibly react with ethanol molecules to produce some byproduct. Finally, the obtained crude product was further purified by column chromatography by using hexane to remove the byproducts. The resulted gray color viscus oil was dried under a vacuum condition to yield the urea bridged dopamine-silane (DPU) precursor [32, 33]. ^{1}H NMR (400 MHz, MeOH-d4): δ 0. 45 (t, 4H, $SiCH_2$), δ 1.03 (t, 18H, CH_2CH_2O), δ 1.62 (t, 4H, $SiCH_2CH_2$), δ 3.65 (t, 4H, NH), δ 6.5–7.8 (m, 3H, aromatic). ^{13}C NMR (400 MHz, MeOH-d4): δ 1.84 (CH_2Si), δ 10.5 (CH_3), δ 15.8 (CH_2), δ 35.8 (O–H), δ 60.2 (aromatic), δ 122.7 (C=O). FTIR (KBr): 1451 cm^{-1} (υ_{N-H}), 1736 cm^{-1} ($\upsilon_{C=O}$), 1465 cm^{-1} (υ_{O-H}), 1512 cm^{-1} ($\upsilon_{C=C}$), 2882, 2927 cm^{-1} (υ_{C-H}) (Scheme 1, step-1).

2.3 Synthesis of DPU organosilica precursors-integrated mesoporous silica hybrid (DPU@MSH) materials

The DPU organosilica precursors-integrated mesoporous silica hybrid (DPU@MSH) material was synthesized by sol–gel hydrolysis and co-condensation method under ammonia catalyzed basic medium [34]. Typically, 0.6 g of CTAB was dissolved in 160 mL deionized water and 3 g of ammonia solution was added magnetically stirred for 30 min. To this, the premixed solution of DPU (precursor A) and TEOS (precursor B), to afford a molar percentage of DPU/TEOS + DPU = 20 mol% was then added dropwise into the surfactant solution under vigorous stirring. The obtained reaction mixture was then stirred for 12 h at 45 °C and further stirred for another 24 h at 85 °C. The obtained solid suspension was filtered and washed with deionized water, and then dried at 60 °C. The as-synthesized material was labelled as DPU@(CTAB)-MSH (Scheme 1, step-2).

2.4 Fabrication of magnetic nanoparticles onto the outer surface of the DPU@(CTAB)-MSH materials

To integrate the magnetic nanoparticles onto the outer surface of the DPU@(CTAB)-MSH nanoparticles, firstly, we modified the outer surface of the DPU@(CTAB)-MSH silica materials by DPU organosilane units. To immobilize the DPU units, about 0.1 g of the as-synthesized DPU@(CTAB)-MSH samples were dispersed in 50 mL of dry toluene. To this, 2 mL (0.2 M) of DPU precursor solution was added dropwise under magnetic stirring and further refluxed at 80 °C for 24 h. The resulted samples were collected by centrifugation and washed with toluene and ethanol, and dried at 60 °C. The obtained samples were labelled as DPU/DPU@(CTAB)-MSH materials (Scheme 1, step-3). Secondly, the magnetic nanoparticles were grown onto the outer surface of the DPU/DPU@(CTAB)-MSH materials by dispersing 0.1 g of DPU/DPU@(CTAB)-MSH materials in 100 mL of deionized water. To this, approximately 50 mg (0.07 mmol) of $FeCl_3$ solution was added slowly under vigorous stirring and further stirred for 15 min to form Fe^{3+}-dopamine complex (Scheme 1, step-4) [35, 36]. Thirdly, the complexed Fe^{3+} ions were then reduced into magnetic iron oxide (Fe_3O_4) nanoparticles by adding hydrazine (25 µmol) as reducing agent and the resulted suspension mixture was then transferred into an autoclave (100 mL) and heated at 150 °C for 12 h [37–39]. The obtained suspension was separated by external magnet, washed with water to remove the non-magnetic silica particles and then dried at 60 °C. The obtained sample was labelled as Fe_3O_4@DPU@(CTAB)-MSH materials (Scheme 1, step-5). Finally, the occluded CTAB surfactant from the Fe_3O_4@DPU@(CTAB)-MSH material was extracted by solvent extraction process by using alcoholic solution of ammonium nitrate. For solvent extraction process, the alcoholic solution of ammonium nitrate (approximately 50 mg of ammonium nitrate dissolved in 80 mL ethanol) was used, and the extraction process was repeated three times at 60 °C for 3 h and finally dried at 60 °C. The obtained CTAB-free sample was labelled as magnetic mesoporous silica hybrid (Fe_3O_4@DPU@MSH material (Scheme 1, step-6).

2.5 Characterization

The low-angle and wide-angle X-ray diffraction (XRD) patterns were measured on X'Pert-MPD system (Philips, Almelo, Netherlands) X-ray diffractometer with Cu Kα radiation. Fourier transform-infrared (FTIR) spectra of the materials were analyzed on a Perkin-Elmer 1320 FTIR spectrometer using KBr pellet. Field emission transmission electron microscopy (FETEM) images were obtained from JEOL JEM-2100F at 200 kV. N_2 adsorption–desorption isotherms were measured at a liquid nitrogen temperature (− 196 °C) using a Nova 4000e surface area analyzer. The specific surface area was calculated by the Brunauer–Emmett–Teller (BET) method. The magnetic behavior of the sample was analyzed by using superconducting quantum interference device (SQUID) at 300 K on a quantum design vibrating sample magnetometer (VSM) (MPMS XL, 7.0). The magnetic heating profiles and the specific absorption rate (SAR) of the samples were measured on a magnetic hyperthermia analyzer (Nanoscale Biomagnetics, Spain) under an AC

magnetic field at f = 409 kHz and at H = 180 Gauss. Particle size distribution of the sample was measured by dynamic light scattering using Beckman Coulter, LS 13,320 particle size analyzer. Elemental analysis (%C, %N, %O and %S) was performed using a Perkin Elmer 2400 series II CHN Elemental analyzer. Inductively coupled plasma (ICP) (Optima 700 DV, Perkin Elmer) measurement was performed to determine the content of the Fe_3O_4 nanoparticles onto the silica samples. Fluorescence microscopic images were obtained on a Leica DMI 3000B fluorescence spectrometer.

2.6 Drug loading into the Fe_3O_4@DPU@MSH material

For loading and in vitro drug release experiments, a model anticancer drug 5-fluorouracil (5-FU) and a model dye rhodamine 123 (Rh123) were chosen to determine the drug loading and release behavior. For cargo loading, approximately 50 mg of the Fe_3O_4@DPU@MSH samples were dispersed in 5-FU drug solution (5 mL, 25 mg/mL water) or Rh123 dye solution (5 mL, 2 mg/mL EtOH), respectively, under sonication for 10 min and the suspensions were magnetically stirred for 24 h. After then, the drug-loaded samples were separated and washed with 5 mL of water to remove the surface adhered drug molecules (Scheme 2). The washing solutions were combined with supernatant to determine the loading efficiency of 5-FU and Rh123 by using UV–Vis spectrometry at 265 nm for 5-FU or at 512 nm for Rh123 by using the following equations:

$$\text{Loading efficiency (\%)} = \frac{\text{Weight of drug in sample}}{\text{Weight of drug injected}} \times 100$$

$$\text{Loading content (\%)} = \frac{\text{Weight of drug in sample}}{\text{Weight of sample taken}} \times 100$$

From the above equation, the loading efficiency and loading content of the 5-FU was estimated to be approximately ~ 78 and ~ 22.3%. Similarly, the loading efficiency and loading content of Rh123 was determined to be ~ 63 and ~ 14.6%, respectively.

2.7 Magnetic heating efficiency of the Fe_3O_4@DPU@MSH material

The magnetic heating efficiency of the pristine Fe_3O_4 NPs and the synthesized Fe_3O_4@DPU@MSH material was determined by using an alternating magnetic current hyperthermia instrument operating at the applied magnetic field frequency f = 409 kHz and the applied magnetic amplitude H = 180 Gauss. To perform the hyperthermia experiments, Fe_3O_4@DPU@MSH samples were dispersed in water at a concentration of 30 mg/mL and positioned in the middle of the coil (three turns copper coil with 6 mm thickness and 65 mm of inner radius) under an AMF. Under applied magnetic field, the temperature increment of the samples were continuously logged using fiber optic probe placed in the center position of the vial containing Fe_3O_4 NPs or Fe_3O_4@DPU@MSH sample suspension. The temperature measurement was started when the suspension was stabilized to room temperature and the measurement time was limited to 10 min. The specific absorbance rate (SAR) was determined to evaluate the magnetic hyperthermia heating efficiency of the Fe_3O_4@DPU@MSH materials.

2.8 In vitro drug release experiments in the absence of alternating magnetic fields (AMF)

We have performed six experimental sets with different pH (pH 7.4 and 5.0) and different temperature [room temperature (25 °C), physiological body temperature (37 °C) and hyperthermia temperature (45 °C)] conditions, respectively, to evaluate the pH-stimuli responsive drug release behaviour of Fe_3O_4@DPU@MSH material. We have chosen two different pH conditions such as physiological pH (pH 7.4) and tumour environmental pH (pH 5.0) as pH stimuli. At the same time, three different temperature conditions such as room temperature (25 °C), physiological body temperature (37 °C) and hyperthermia temperature (45 °C) were selected to mimic temperature stimuli. To perform the in vitro drug release experiments, in each temperature set, one sample was maintained at physiological pH (pH 7.4) and other samples were maintained at acidic pH (pH 5.0) conditions.

For in vitro drug release experiments, approximately 50 mg of 5-FU loaded Fe_3O_4@DPU@MSH/5-FU sample or Rh123 loaded Fe_3O_4@DPU@MSH/Rh123 sample was placed in a dialysis membrane (MWCO 12 kDa) and placed in 25 mL of PBS solution with appropriate pH conditions under gentle magnetic stirring. The release behaviour of 5-FU or Rh123 was progressively monitored by using UV–Vis spectrometry by measuring the absorbance maximum values of the released 5-FU at 265 nm or Rh123 at 512 nm, respectively. At pre-determined time intervals, approximately 2 mL of the sample was withdrawn from the release medium and the absorbance was measured.

2.9 In vitro cytocompatibility of the Fe_3O_4@DPU@MSH material

The in vitro cytotocompatibility of the synthesized Fe_3O_4@DPU@MSH material was evaluated by using MDA-MB-231 cell line. For cell seeding, the Fe_3O_4@DPU@MSH materials were dispersed in Dulbecco's modified eagle's medium (DMEM) with different concentrations (25–100 µg/mL). Then, the cells were seeded in 96-well plates (1×10^4 cells per well) and cultured in DMEM media supplemented with

10% foetal bovine serum and 1% antibiotic solution at 37 °C in a humidified 5% CO_2 atm. After 24 h incubation, 20 µL of the 3-(4,5-dimethylthiazol-2-yl)-2,5-diphenyltetrazolium bromide (MTT) solution was added to each well and then the optical density (OD) was determined at 570 nm. Cell viability was calculated using the following equation [40].

$$\text{Cell viability (\%)} = \frac{\text{OD of treated cells}}{\text{OD of control cells}} \times 100$$

where $OD_{treated}$ represents the OD value obtained from the cells treated with the 5-FU-loaded Fe_3O_4@DPU@MSH/5-FU nanoparticles for 24 h. The $OD_{control}$ represents the OD value obtained from the cells treated without nanoparticles treatment.

2.10 Intracellular uptake efficiency of the Fe_3O_4@DPU@MSH material

The intracellular uptake efficiency of the Fe_3O_4@DPU@MSH materials was examined using MDA-MB-231 cell line and visualized by fluorescence microscope. For this experiment, approximately 10 µg/mL of the Rh123 loaded Fe_3O_4@DPU@MSH/Rh123 sample was incubated with MDA-MB-231 cells. After 6 h incubation period, the cells were attached to the bottom of petri dish and the cells were washed three times using PBS solution to remove the unattached nanoparticles and dead cells and then the cells were fixed with 4% paraformaldehyde for 15 min. Finally, the cells were washed with PBS for three times and then the cells were observed under fluorescence microscope (Leica DMI 3000B fluorescence spectrometer).

3 Results and discussion

3.1 Characterization of the Fe_3O_4@DPU@MSH material

Figure 1a shows the low-angle XRD pattern of the magnetic mesoporous silica Fe_3O_4@DPU@MSH material. As shown in Fig. 1a, the Fe_3O_4@DPU@MSH material shows XRD peak at $2\theta = 2.4°$ with d-spacing of 3.9 nm, suggested the presence of mesopores in the synthesized Fe_3O_4@DPU@MSH material [29]. Similarly, the wide-angle XRD pattern (Fig. 1b) shows a broad peak in the range at $2\theta = 20–30°$ suggested the formation of mesoporous silica matrix. In addition, the wide-angle XRD pattern shows well-resolved diffraction peaks at $2\theta = 29.9°$, 35.4°, 43.2°, 47.3°, 57.1° and 63.2° were assigned to [220], [311], [400], [422], [511] and [440] reflection planes which supported the formation of the crystalline Fe_3O_4 nanoparticles which present onto the outer surface of the Fe_3O_4@DPU@MSH materials. The obtained XRD patterns agrees well with the standard XRD patterns of the magnetite listed in the XRD standard card (JCPDS 85-1436). The low-angle and higher-angle XRD analysis results evidenced the formation of mesoporous silica materials and the formation of magnetic Fe_3O_4 nanoparticles onto the outer surface of the Fe_3O_4@DPU@MSH materials with well-retained crystalline structure.

FTIR analysis was performed to verify the integrated DPU organosilica precursors into the Fe_3O_4@DPU@MSH materials. As shown in Fig. 2, the vibration bands at 1062 and 963, 463 and 3428 cm^{-1} were assigned to Si–O–Si, Si–OH, Si–O and surface hydroxyl (–OH) groups, respectively [41]. The stretching modes at 2873 and 2960 cm^{-1} were assigned to the symmetric and asymmetric C–H

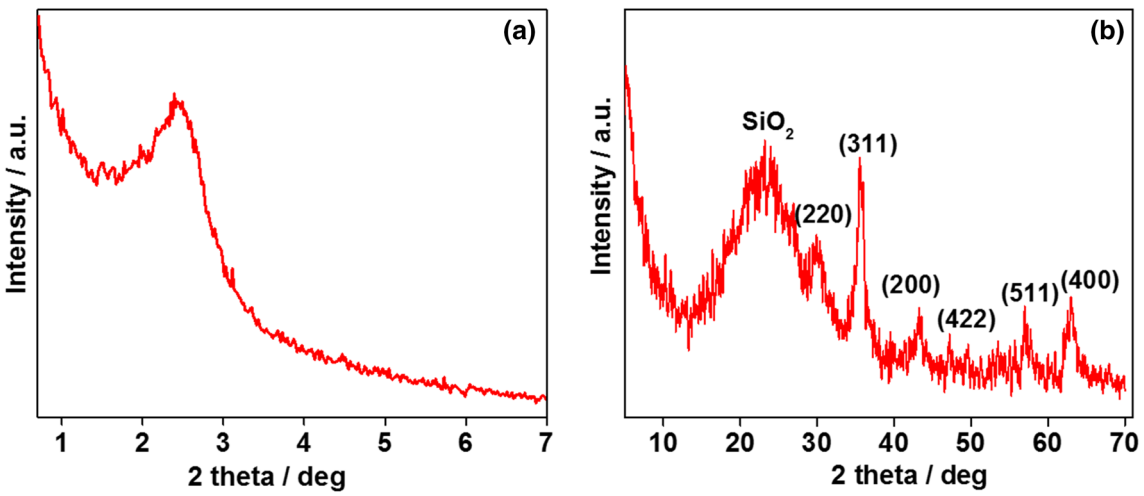

Fig. 1 **a** Low-angle and **b** wide-angle XRD patterns of the Fe_3O_4@DPU@MSH material

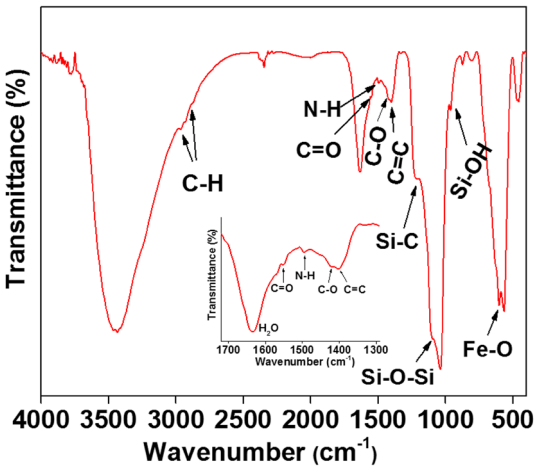

Fig. 2 FTIR spectrum of the Fe_3O_4@DPU@MSH materials

stretching vibrations of propyl carbon chains present in the integrated DPU organosilane precursors. Furthermore, two characteristic bands at 1495 and 1562 cm^{-1} are ascribed to the C=O and N–H groups of the urea groups and the additional bands at 1426 and 1398 cm^{-1} were assigned to C–O, C=C vibration frequencies arose from dopamine part of DPU organosilica units [42]. In addition, the typical characteristic band appeared at 568 cm^{-1} typical for Fe-O stretching vibration band which further supports that the existence of magnetic Fe_3O_4 nanoparticles onto the outer surface of the Fe_3O_4@DPU@MSH materials. Moreover, a broad peak at 1215 cm^{-1} for Si–C stretching confirms that the existence of DPU organosilane units into the mesopore channels of the silica materials. The FTIR result confirms that the presence of the DPU organosilane groups as well as the existence of the magnetic Fe_3O_4 nanoparticles in the Fe_3O_4@DPU@MSH materials.

FETEM analysis was used to observe the presence of mesopore channels as well as the formation of the magnetic Fe_3O_4 nanoparticles onto the outer surface of the silica pore wall. Figure 3a, b, d and e shows the low and high magnified TEM images of the Fe_3O_4@DPU@MSH materials. From the TEM images, it was observed that the presence of mesopores in the Fe_3O_4@DPU@MSH material. Furthermore, it can be seen that the dark black spots highlighted in arrows (Fig. 3b, d and e) which confirms that the existence of the Fe_3O_4 nanoparticles onto the outer surface of the silica pore walls. The material consists of several individual Fe_3O_4 nanoparticles

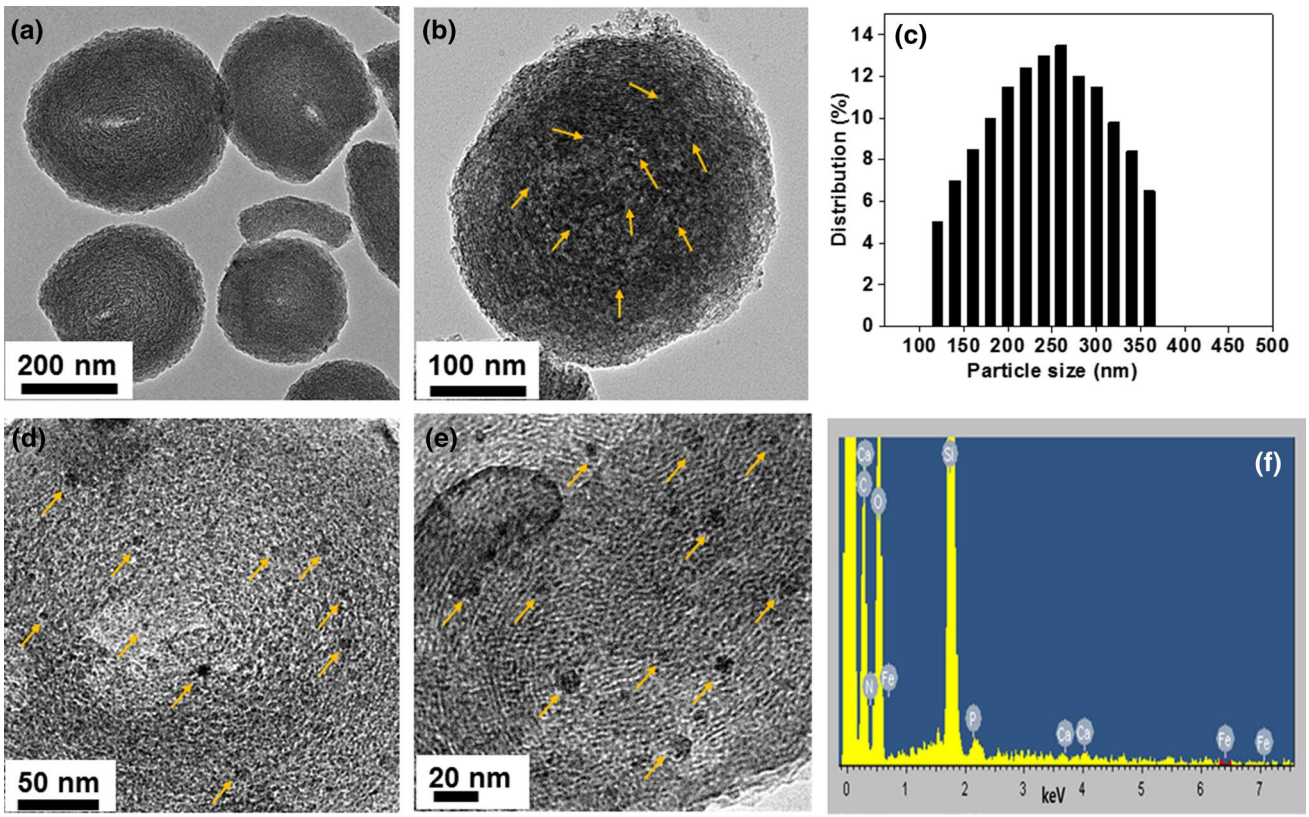

Fig. 3 Low and high magnified FETEM images **a, b** and **d, e** of the Fe_3O_4@DPU@MSH material. High magnified images **d, e** shows the presence of magnetic Fe_3O_4 nanoparticles pointed in arrows. **c** Particle size distributions of the Fe_3O_4@DPU@MSH material. **f** EDX spectrum of Fe_3O_4@DPU@MSH material

in the Fe_3O_4@DPU@MSH material with the average particle size is approximately ~ 5–10 nm, which were dispersed onto the outer surface of the silica walls (Fig. 3d, e). TEM images are similar with the reported magnetic silica materials in the literatures [43–45]. The obtained TEM results are in agreement with the wide-angle XRD patterns of Fe_3O_4@DPU@MSH material. Further, the energy-dispersive X-ray spectroscopy (EDS) analysis (Fig. 3f) of the Fe_3O_4@DPU@MSH represents the presence of some elements such as silicon (Si), iron (Fe), carbon (C), oxygen (O) and nitrogen (N) in the body of the Fe_3O_4@DPU@MSH material. In other words, this illustrates that the Fe_3O_4@DPU@MSH material is composed of 38% of silica, 28% of iron, 32% of oxygen and 4.8% of nitrogen which confirms the existence of iron nanoparticles in the Fe_3O_4@DPU@MSH material. This result is also consistent with the result of X-ray diffraction analysis. TEM images show that the average particle size of the Fe_3O_4@DPU@MSH nanomaterial is ~ 150–350 nm size and the particles are almost in spherical shape (Fig. 3a, b). In addition, the particle size distribution of the Fe_3O_4@DPU@MSH materials was determined by dynamic light scattering (DLS) measurement using water as dispersion medium. From the DLS data (Fig. 3c), the average particle size of the Fe_3O_4@DPU@MSH material was estimated in the range between 150 and 350 nm.

Figure 4a, b shows N_2 adsorption–desorption isotherm and pore size distribution curves of Fe_3O_4@DPU@MSH materials. As observed in Fig. 4, the material shows type IV isotherm curve which represent the formation of mesoporous silica materials. The BET surface area, pore size and pore volume of the Fe_3O_4@DPU@MSH samples were calculated to be 386 m^2/g, 4.2 nm and 0.52 cm^3/g, respectively (Table 1). The thermal stability of the synthesized Fe_3O_4@DPU@MSH materials was determined by thermogravimetric analysis (Fig. 5a, b). As shown in Fig. 5, the sample shows an initial weight loss of approximately 1.6 wt% occurs at 100 °C due to the physisorbed water or moisture. The Fe_3O_4@DPU@MSH material shows the second weight loss, approximately 22.3 wt% occurs in the temperature range from 101 to 650 °C which is corresponding to the decomposition of the DPU organosilane functional derivatives which were integrated onto the inner and outer surface of the silica pore walls. In addition, the third weight loss occurs beyond 650 °C, which indicates the decomposition of inorganic silica matrix. The TGA results show that the weight loss occurs approximately 22.3 wt% suggesting that a considerable amount of DPU organosilane functional groups were integrated with the mesoporous silica Fe_3O_4@DPU@MSH materials. The carbon and nitrogen contents of the extracted samples were analysed quantitatively by elemental analysis.

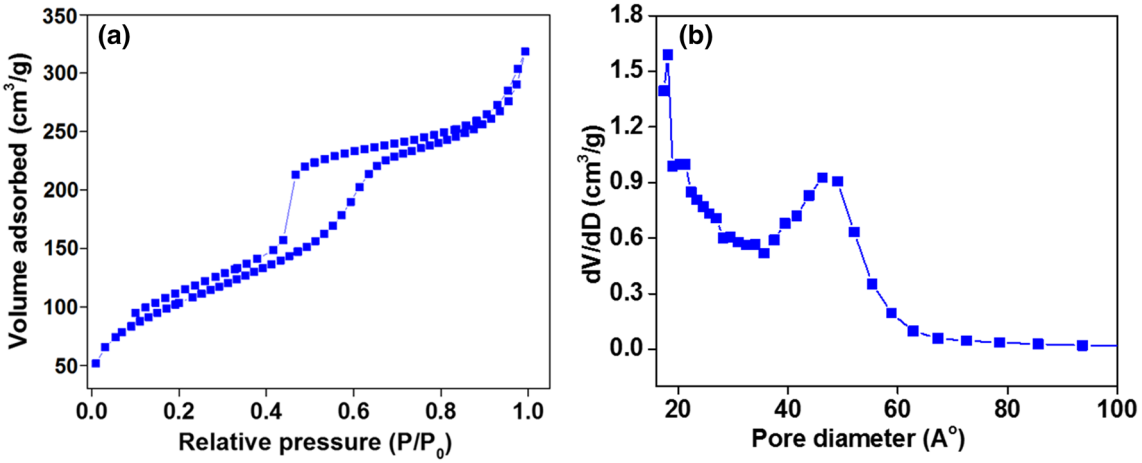

Fig. 4 **a** N_2 adsorption–desorption isotherm and **b** pore size distribution of Fe_3O_4@DPU@MSH material

Table 1 Structural properties of the Fe_3O_4@DPU@MSH materials

Material	Fe_3O_4@DPU in the pore walls by EA (mol/g)	Fe_3O_4 by ICP-EOS (wt%)	d_{100} (nm)	Surface area (m^2/g)	Pore size (nm)	Pore volume (cm^3/g)	Cargo loading efficiency (%)	
							5-FU	Rh123
Fe_3O_4@DPU@MSH	13.8	23.92	3.9	386	4.2	0.52	~ 78	~ 63

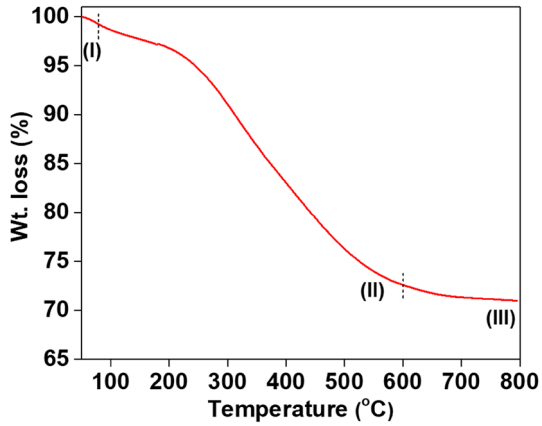

Fig. 5 TGA curve of Fe_3O_4@DPU@MSH materials

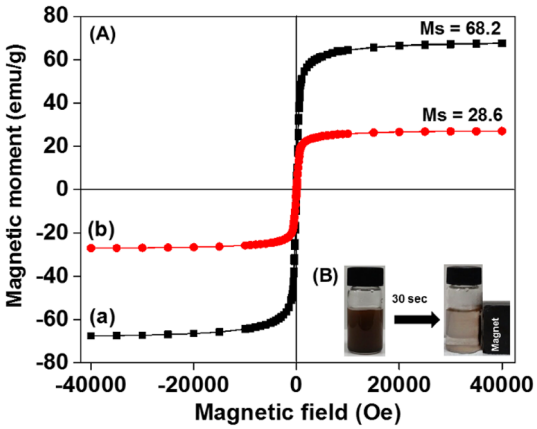

Fig. 6 **A** Magnetization curves of **a** Fe_3O_4 nanoparticles and **b** Fe_3O_4@DPU@MSH materials and **B** photographs of aqueous suspensions of Fe_3O_4@DPU@MSH material (left) and after magnetic attraction within 30 s (right)

The elemental analysis data for the Fe_3O_4@DPU@MSH materials demonstrates the presence of C, N, H and O atoms, which confirms the existence of the DPU organosilane functionalities in the silica network. From the EA data, the amount of functionalised DPU organosilane groups was calculated to be about ~ 13.8 mol/g of the Fe_3O_4@DPU@MSH material (Table 1). In addition, the formation of magnetic Fe_3O_4 nanoparticles was quantified by inductively coupled plasma optical emission spectroscopy (ICP-OES) method. To perform this, the Fe_3O_4@DPU@MSH sample was dissolved in hydrofluoric acid (4 wt% in water) and stirred for 4 h. Then, the obtained solution was used for the quantification of iron present in the samples using standard Fe solution at known concentration. From the ICP-OES analysis data, the content of the magnetic nanoparticles present onto the silica pore walls of the Fe_3O_4@DPU@MSH materials was determined to be 23.92 wt% (Table 1).

3.2 Magnetisation and magnetic heating efficiency of the Fe_3O_4@DPU@MSH material

The magnetic behaviour of the pristine Fe_3O_4 nanoparticles and the Fe_3O_4@DPU@MSH materials were determined by superconducting quantum interference device (SQUID) and by vibrating sample magnetometer (VSM). Figure 6Aa, b shows the magnetisation curves of pristine Fe_3O_4 nanoparticles and Fe_3O_4@DPU@MSH materials with magnetic saturation values of 68.2 and 28.6 emu/g, respectively. Moreover, the Fe_3O_4@DPU@MSH materials showed no hysteresis in their room temperature magnetization curve implies that the synthesized Fe_3O_4@DPU@MSH nanomaterial possesses superparamagnetic property [46]. The magnetic behaviour of the Fe_3O_4@DPU@MSH was further confirmed by the following observation. About 10 mg of the sample was dispersed in PBS medium under sonication and then placed near a magnet bar. The material showed rapid attraction towards the external magnet bar within 30 s when the magnet bar was placed near the glass vial (Fig. 6B, inset). This observation supports the hypothesis that the Fe_3O_4@DPU@MSH nanomaterial possesses magnetic property and it could be directed by external magnetic field and hence, it is desirable for external magnetic field driven targeted drug delivery applications in cancer therapy.

The magnetic heating capacity of the pristine Fe_3O_4 and Fe_3O_4@DPU@MSH materials was evaluated by magnetic hyperthermia instrument (Scheme 2). For magnetic hyperthermia experiments, approximately 30 mg/mL concentration of the pristine Fe_3O_4 NPs or Fe_3O_4@DPU@MSH samples were dispersed in water and exposed to an alternating magnetic field with the applied magnetic field f = 409 kHz and the applied magnetic field strength H = 180 Gauss. The magnetic heating profiles of the pristine Fe_3O_4 nanoparticles and Fe_3O_4@DPU@MSH materials are shown in Fig. 7a, b. As shown in Fig. 7a, b, the temperature raised from 25 to 67 and 56 °C, respectively, for pristine Fe_3O_4 and Fe_3O_4@DPU@MSH within 10 min. Furthermore, the Fe_3O_4@DPU@MSH sample reached the hyperthermia temperature range (45 °C) within approximately 4.5 min when applying the magnetic field frequency f = 409 kHz, suggesting that the Fe_3O_4@DPU@MSH material has the capacity to reach the hyperthermia temperature region within a very short time under an alternating magnetic field. The magnetic hyperthermia heating experiment result evidenced that the Fe_3O_4@DPU@MSH material could be applied for hyperthermia treatment in cancer therapy. Approximately, 30 mg/mL of the Fe_3O_4@DPU@MSH sample was used to determine the heating capacity. This concentration is relatively lower than the reported literatures. For example, Jordan et al. reported that the average concentration of magnetic nanoparticles of approximately 112 mg/mL was used for clinical

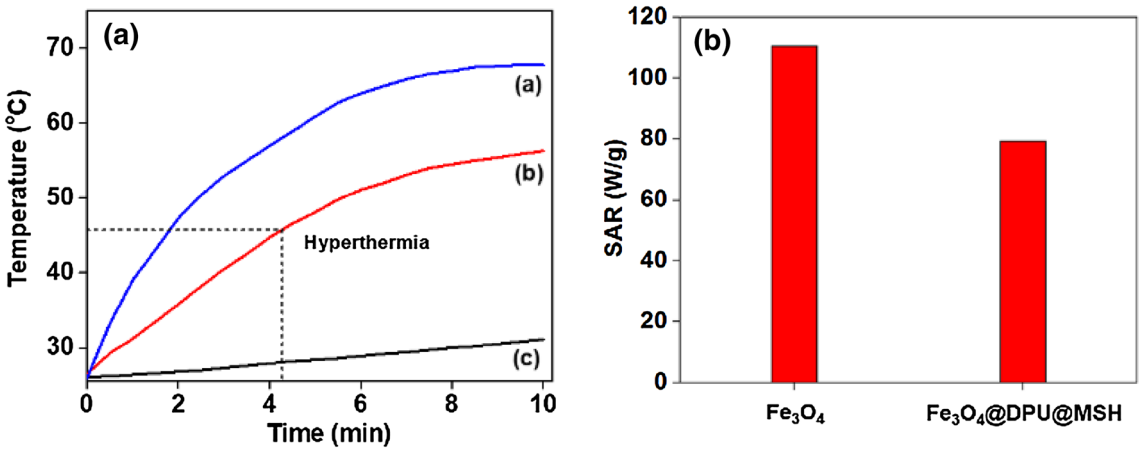

Fig. 7 **A** Magnetic thermal response curves of **a** pristine Fe_3O_4 nanoparticles and **b** Fe_3O_4@DPU@MSH materials dispersed in water at a concentration of 10 mg/mL and **c** water were subjected to an alternating magnetic field (f = 409 kHz and H = 180 Gauss). **B** The SAR values of pristine Fe_3O_4 nanoparticles and Fe_3O_4@DPU@MSH materials under magnetic field frequency f = 409 kHz and applied magnetic field H = 180 Gauss

trials [47–49]. The magnetic heating capacity of the pristine Fe_3O_4 and Fe_3O_4@DPU@MSH materials were evaluated by specific absorption rate (SAR) by normalizing the heating efficiency in W/g by using the following formula [50].

$$\mathrm{SAR(W/g)} = \left(C_w/m\right)\left(dT/dt\right)$$

where C_w is the specific heat capacity of suspension ($=4.186\ \mathrm{J\ g^{-1}\ °C^{-1}}$), m is the magnetic material concentration in suspension; dT/dt is the slope of temperature versus time graph. The slope of the dT/dt was calculated by taking into account only the first 60 s. The calculated SAR values for pristine Fe_3O_4 and Fe_3O_4@DPU@MSH material are 110.5 W/g and 79.3 W/g, respectively (Fig. 7B). The calculated SAR value of the Fe_3O_4@DPU@MSH material was lower than the SAR value of the pristine Fe_3O_4 nanoparticles; however, the synthesized Fe_3O_4@DPU@MSH material may be useful for the combined AMF triggered drug delivery applications in cancer treatments.

3.3 Drug loading and in vitro drug release study

The existence of urea (–NH–CO–NH–) groups and the dopamine units present inside the mesopore channels of the Fe_3O_4@DPU@MSH material serves as binding sites for drug molecules. To determine the synthesized Fe_3O_4@DPU@MSH material is desirable for drug carrier, we have chosen 5-FU as a model anticancer drug and Rh123 as model cargo. We chose 5-FU as a model anticancer drug because it can firmly interact with the drug binding sites of urea (–NH–CO–NH–) and dopamine groups present in the mesopore channels through multiple hydrogen bonding interactions [33] and the possible hydrogen bonding/electrostatic interactions with surface silanol groups. Owing to the small size of 5-FU molecules, it is possible to load high amounts of the drug into the Fe_3O_4@DPU@MSH materials. Similarly, the Rh123 was chosen as a model drug to prove that the synthesized Fe_3O_4@DPU@MSH materials have the ability to loading/release of a range of other drug molecules. The Rh123 can be loaded into the Fe_3O_4@DPU@MSH through hydrogen bonding interaction between Rh123 and the urea and dopamine functionalities present in the mesoporous silica material. Generally, the amount of drug loaded into the drug carrier and the release of loaded drugs into the desired sites are considered to be an important factors to improve the specific accumulation of drugs in the desired sites and to reduce the side effects to the normal tissues. In this concern, the Fe_3O_4@DPU@MSH material could be applied as drug carriers for loading and release of drugs in a controlled manner through the protonation of drug molecules and the drug binding sites induced by the intracellular acidic pH environments (Scheme 2).

3.4 In vitro drug release from the Fe_3O_4@DPU@MSH material as a function of combined pH and temperature stimuli

To evaluate the in vitro drug release efficiency of the Fe_3O_4@DPU@MSH material, we have used the combined pH and temperature stimuli to mimic the intracellular pH and hyperthermia temperature stimuli conditions. To mimic the temperature stimuli condition, in this study we used water bath to maintain the appropriate temperature (25, 37 and 45 °C, respectively). In this study, we have performed six sets of experiments. For this purpose, we chose two different pH conditions such as physiological pH (pH 7.4) and tumour environmental pH (pH 5.0), and three different

temperature conditions: (i) room temperature (25 °C), (ii) physiological body temperature (37 °C), and (iii) hyperthermia temperature condition (45 °C), respectively. As shown in Fig. 8Aa, b, all the 5-FU and Rh123 release profiles had two stages of release behaviour, that is first an initial rapid release followed by sustained release behaviour. As observed in Fig. 8Aa, approximately, 13, 19.4 and 24% of the 5-FU were released after 24 h, under physiological pH and three different temperature (pH 7.4/25, 37 and 45 °C) conditions. In contrast, the 5-FU release were more enhanced and approximately 76.3, 81.5 and 90.5% of 5-FU were released at higher acidic pH (pH 5.0) and at three different temperature (pH 5.0/25, 37 and 45 °C) conditions, respectively, after 24 h release period (Fig. 8Aa). Similar release behaviour was observed for the Rh123 at different stimuli conditions. In Fig. 8Ab, the Rh123 release profiles was also showed two stage of release behaviour such as an initial burst release followed by the second controlled release. Approximately, 18.8, 21.5 and 24.6% of Rh123 release were observed after 24 h duration, at physiological pH and three different temperature (pH 7.4/25, 37 and 45 °C) conditions. On the other hand, an increased Rh123 release were observed and approximately 71.2, 79.5 and 92.8% were released at acidic pH (pH 5.0) and at three different temperature (pH 5.0/25, 37 and 45 °C), respectively (Fig. 8Ab). As shown in Fig. 8Aa, b, the 5-FU and Rh123 release were higher at 37 and 45 °C as compared to 25 °C. Approximately 81.5 and 90.5% of 5-FU were released and approximately 79.5 and 92.8% of Rh123 release were observed at 37 and 45 °C, respectively and at acidic pH (pH 5.0) conditions after 24 h release period. The maximum release of 5-FU and Rh123 were achieved when combining both the acidic pH (pH 5.0) and hyperthermia temperature (45 °C) stimuli (Fig. 8Aa, b). The prominent role of the combined pH and temperature stimuli can be explained as follows. Firstly, under acidic pH conditions, the drug molecules and the drug binding urea and dopamine groups present in the mesoporous silica surfaces undergo protonation. An electrostatic repulsive force occurs between the protonated drug molecules and the drug binding urea (–NH–CO–NH–), dopamine (Ph-$(OH)_2$) functional sites which induce the

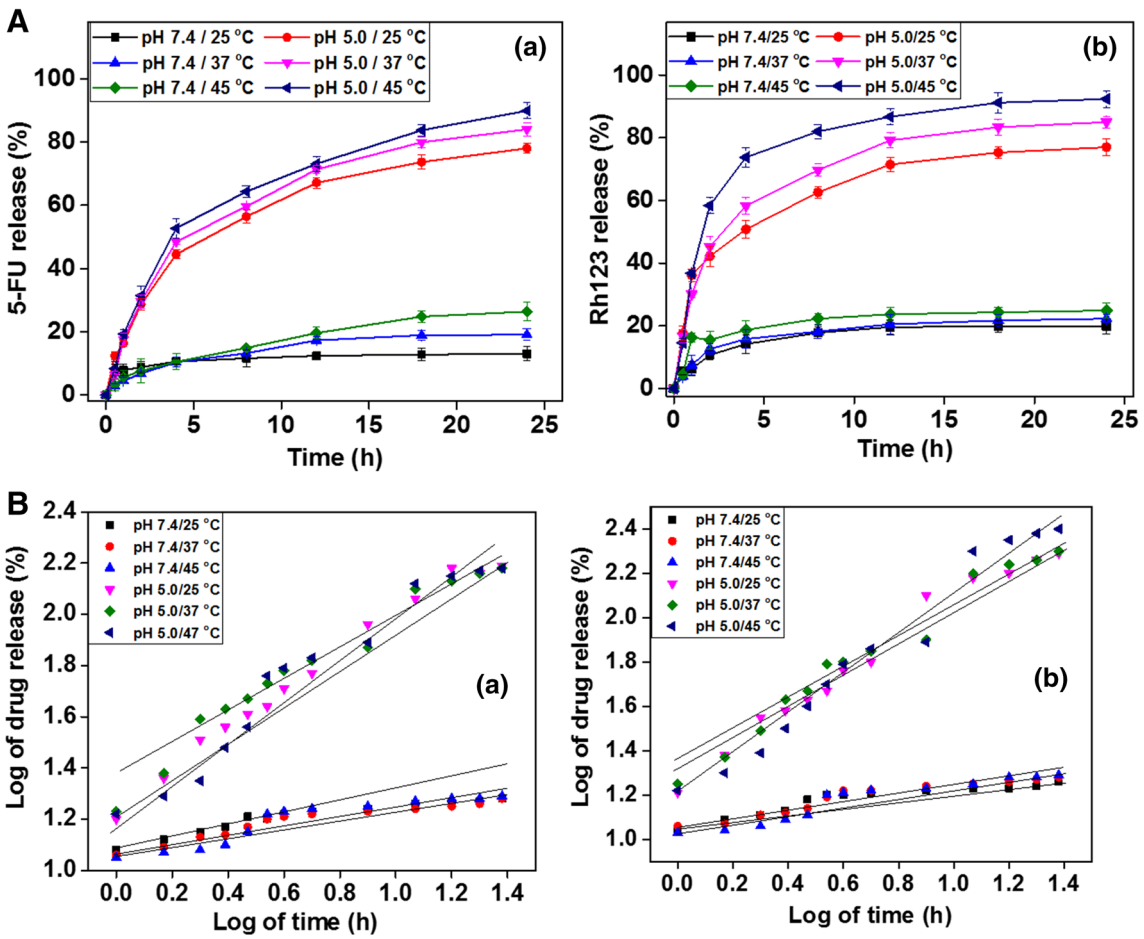

Fig. 8 **A** In vitro release of **a** 5-FU and **b** Rh123 from the Fe_3O_4@DPU@MSH materials under the combined pH (pH 7.4 and 5.0) and temperature (25, 37 and 45 °C) stimuli. **B** Fitting the 5-FU and Rh123 release at different pH/temperature conditions to Korsmeyer–Peppas model

diffusion of drug molecules from the mesopore channels of the Fe_3O_4@DPU@MSH material [45]. Secondly, the temperature stimuli can increase the solubility of the drug molecules to a certain extent in the aqueous medium. Also, the temperature stimuli can accelerate the diffusion of drug molecules from the mesopore channels. Thus, an enhanced drug delivery efficiency can be attained when combining both the acidic pH and hyperthermia temperature (45 °C) stimuli. Therefore, the obtained experimental results supports that the Fe_3O_4@DPU@MSH material could be effectively utilized for the combined pH and temperature stimuli-responsive drug delivery applications in cancer therapy.

The Korsmeyer–Peppas equation is often used to explain the drug release mechanism from the nanomaterials. The in vitro release data was plotted as a log cumulative percentage of drug release vs log time (Fig. 8Ba, b).

$$M_t/M_\infty = Kt^n$$

where M_t/M_∞ is a part of drug released at time t, K is the rate constant, and n is the release exponent. The "n" values for Korsmeyer–Peppas model have been determined from the slope of the log (Mt/M∞) vs. log t plot and the obtained values (<4.5) suggesting that the drug release mechanism is predominantly diffusion controlled mechanism [51].

3.5 In vitro cytotoxicity of Fe_3O_4@DPU@MSH material

The cytocompatibility of any drug carrier is considered to be an important factor to be utilized them for drug delivery applications. The MTT assay analysis was performed on MDA-MB-231 cell line to evaluate the cytotoxicity of the Fe_3O_4@DPU@MSH material. For this experiment, the Fe_3O_4@DPU@MSH without drug loading and the anticancer drug 5-FU (50 µg/mL) loaded Fe_3O_4@DPU@MSH/5-FU samples were studied with the 5-FU as a positive control. As observed in Fig. 9, the Fe_3O_4@DPU@MSH sample showed more than 95% of the MDA-MB-231 cell were viable even in the concentration of 50 µg/mL, which evidenced the synthesised Fe_3O_4@DPU@MSH materials is biocompatible. In contrast, the 5-FU drug (50 µg/mL) loaded Fe_3O_4@DPU@MSH/5-FU sample showed considerably higher cytotoxicity, approximately > 85% of toxicity to MBA-MD-231 cells when the cells were treated with the sample concentration of 50 µg/mL. Similarly, the same concentration of pure 5-FU drug also showed the cytotoxicity approximately ~ 70% to MDA-MB-231 cells. The cell viability were decreased with increasing the concentrations of Fe_3O_4@DPU@MSH/5-FU sample. As shown in Fig. 9, the 5-FU loaded Fe_3O_4@DPU@MSH/5-FU sample showed higher toxicity (> 85%) to MDA-MB-231 cells as compared to the same concentration of free 5-FU drugs. This might be due to the slow and sustained release of loaded 5-FU molecules from the

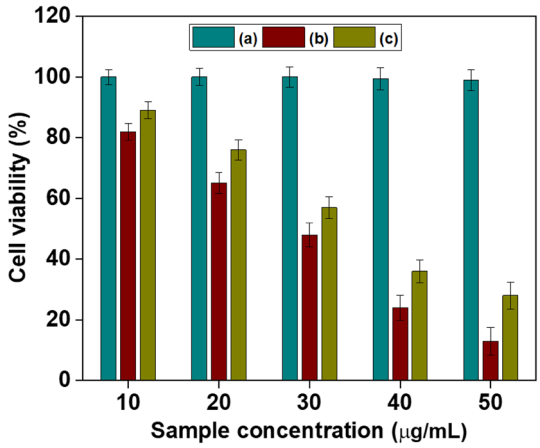

Fig. 9 In vitro cytotoxicity of (*a*) Fe_3O_4@DPU@MSH (*b*) 5-FU loaded Fe_3O_4@DPU@MSH/5-FU and (*c*) free 5-FU against MDA-MB-231 cells after 24 h incubation. (Color figure online)

mesopore channels of the Fe_3O_4@DPU@MSH/5-FU materials. The strong hydrogen bonding and electrostatic interactions between the 5-FU molecules and the drug binding urea and dopamine functional sites present in the mesopore channels of the Fe_3O_4@DPU@MSH materials which controls the release behaviour of loaded drugs [45]. Generally, the free drug molecules are transported into the cells by a passive diffusion mechanism whereas the Fe_3O_4@DPU@MSH/5-FU nanoparticles are internalized into the cells by possible endocytosis mechanism and thus the loaded drug molecules are gradually released from the Fe_3O_4@DPU@MSH/5-FU samples. This result is in agreement with the reported literatures [52]. The experimental results support that the anticancer drug loaded Fe_3O_4@DPU@MSH/5-FU materials can inhibit the cancer cell proliferation to a great extent, and it could be used as a potential magnetically directed drug delivery carrier for targeted cancer therapy.

3.6 Intracellular uptake study

Intracellular uptake of the drug carrier is an important factor in drug delivery applications. The efficient cellular uptake of the drug loaded magnetic silica particles could be beneficial for magnetic hyperthermia therapy due to magnetic local heating in tumor sites and also enhance the chemotherapeutic efficiency by intracellular delivery of loaded drugs. The intracellular uptake behaviour of the Rh123 loaded Fe_3O_4@DPU@MSH/Rh123 material was tested on MDA-MB-231 cells and the uptake efficiency of the sample was monitored by using fluorescence microscopic analysis. For this study, Rh123 loaded Fe_3O_4@DPU@MSH/Rh123 samples with the concentration of 10 µg/mL were dispersed in PBS solution and treated to the MDA-MB-231 cells and incubated for 6 h. After 6 h incubation, the cells were washed with PBS

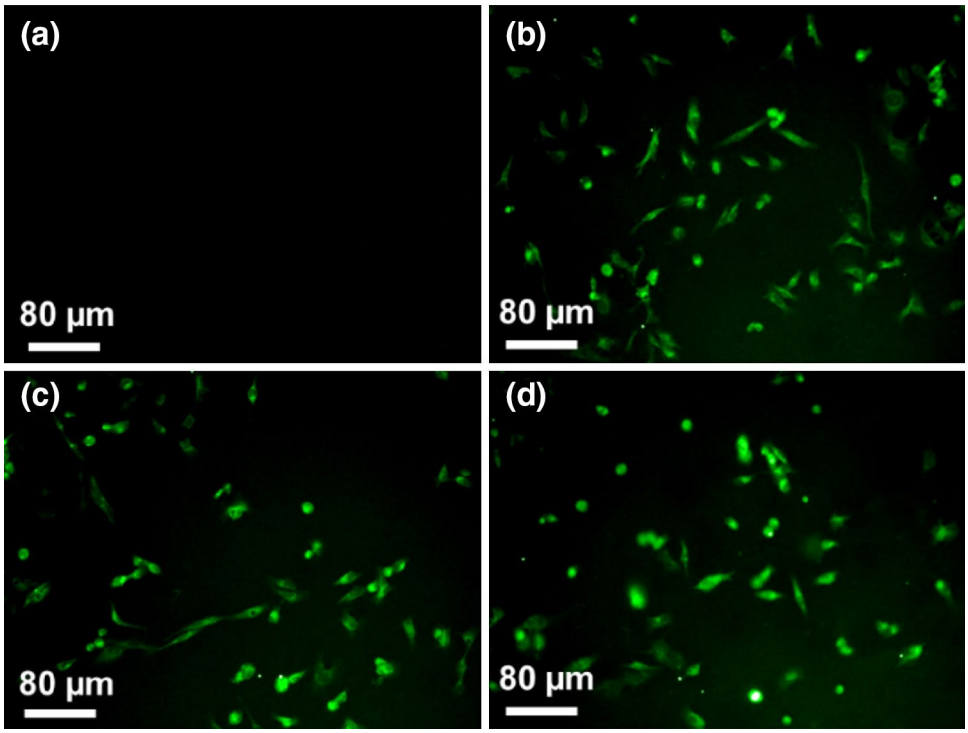

Fig. 10 Fluorescence microscopic images of MDA-MB-231 cancer cells incubated with **a** control and **b**–**d** Rh123 loaded Fe_3O_4@DPU@MSH materials incubated for 6 h

solution and then the images were observed under fluorescence microscope. The fluorescent images were displayed in Fig. 10. As observed in Fig. 10a, no green fluorescence was observed in the control image whereas the Rh123 loaded Fe_3O_4@DPU@MSH/Rh123 sample treated cells showed a clear green fluorescence (Fig. 10b–d). The fluorescent study clearly authenticated that the Fe_3O_4@DPU@MSH/Rh123 nanoparticles were effectively up taken by MDA-MB-231 cells. This results supports that the Fe_3O_4@DPU@MSH materials could be applied as an efficient drug carrier system for local delivery of anticancer agent cancer therapy.

4 Conclusions

In summary, we have synthesized a magnetic mesoporous silica hybrid Fe_3O_4@DPU@MSH materials by combining sol–gel co-condensation method and metal–ligand complex coordination approaches. By this approach, the magnetic Fe_3O_4 nanoparticles were grown onto the outer surface of the mesoporous silica walls without altering mesoporous structural morphology. The synthesized Fe_3O_4@DPU@MSH materials showed almost uniform particles with the average particle sizes approximately 150–350 nm. The Fe_3O_4@DPU@MSH material exhibits mesoporous structure with high surface area, large pore size and pore volume. Owing to the presence of high surface area and the drug binding urea and dopamine functional groups in the Fe_3O_4@DPU@MSH materials showed high drug loading and pH-responsive drug release behavior. In addition, owing to the magnetic Fe_3O_4 nanoparticles present onto the outer surface of the mesoporous silica walls, the Fe_3O_4@DPU@MSH material showed high magnetic heating capacity when applying an alternating magnetic field and have ability to reach the hyperthermia temperature (45 °C) within a very short time, approximately 4.5 min. The model drugs such as 5-FU and Rh123 loaded Fe_3O_4@DPU@MSH sample showed an enhanced drug release behavior about more than 90% under acidic pH-stimuli (pH 5.0) and hyperthermia temperature (45 °C) conditions. In addition, the MTT assay study results support that the Fe_3O_4@DPU@MSH material is biocompatible in the tested concentrations and also the fluorescence microscopic study evidenced that the Fe_3O_4@DPU@MSH particles could be effectively uptake by MDA-MB-231 cells. From all the study results, it could concluded that the synthesized Fe_3O_4@DPU@MSH material would be a promising candidate that may serve as efficient drug carrier for the pH-responsive delivery of anticancer agents in chemotherapy and magnetic hyperthermia agent in thermotherapy applications.

Acknowledgements This research was supported by a Grant from the Marine Biotechnology Program (20150220) funded by the Ministry of Oceans and Fisheries, Republic of Korea.

References

1. D.-E. Lee, H. Koo, I.-C. Sun, R.H. Ryu, K. Kim, I.C. Kwon, Chem. Soc. Rev. **41**, 2656 (2012)
2. R. Abu-Reziq, H. Alper, D.G. Wan, M.L. Post, J. Am. Chem. Soc. **128**, 5279 (2006)
3. A. Faucon, H. Benhelli-Mokrani, F. Fleury, L. Dubreil, P. Hulin, S. Nedellec, T. Doussineau, R. Antoine, T. Orlando, A. Lascialfari, J. Fresnais, L. Lartigue, E. Ishow, J. Colloid Interface Sci. **479**, 139 (2016)
4. M.S. Moorthy, H.-B. Kim, A.-R. Sung, J.-H. Bae, S.-H. Kim, C.-S. Ha, Micropor. Mesopor. Mater. **194**, 219 (2014)
5. Y. Tang, Y. Liu, Y. Qin, Y. Xu, X. Qian, W. Zhu, J. Colloid Interface Sci. **479**, 7 (2016)
6. H. Zhang, Y. Liu, J. Wu, B. Xin, J. Colloid Interface Sci. **476**, 214 (2016)
7. L. Zhang, S.Z. Qiao, Y.G. Jin, Z.G. Chen, H.C. Gu, G.Q. Lu, Adv. Mater. **20**, 805 (2008)
8. J. Fan, W.Q. Shui, P.Y. Yang, X.Y. Wang, Y.M. Xu, H.M. Wang, X. Chen, D.Y. Zhao, Chem.-Eur. J. **11**, 5391 (2005)
9. E. Kartz, I. Willner, Angew. Chem. Int. Ed. **43**, 6042 (2004)
10. J.P. Ge, Q. Zhang, T.R. Zhang, Y.D. Yin, Angew. Chem. Int. Ed. **47**, 8924 (2008)
11. J. Zhou, W. Wu, D. Caruntu, M. Yu, A. Martin, J. Chen, C. O'Connor, W. Zhou, J. Phys. Chem. C **111**, 17473 (2007)
12. J. Kim, J.E. Lee, J. Lee, J.H. Yu, B.C. Kim, K. An, Y. Hwang, C.H. Shin, J.G. Park, J. Kim, T. Hyeon, J. Am. Chem. Soc. **128**, 688 (2006)
13. W. Zhao, J. Shi, H. Chen, L. Zhang, J. Mater. Res. **21**, 3080 (2006)
14. E. Ruiz-Hernandez, A. Lopez-Noriega, D. Acros, I. Izquierdo-barba, O. Terasaki, M. Vallet-Regi, Chem. Mater. **19**, 3455 (2007)
15. Q.H. Min, X.X. Zhang, R.A. Wu, H.F. Zou, J.J. Zhu, Chem. Commun. **47**, 10725 (2011)
16. F. Caruso, M. Spasova, A. Susha, M. Giersig, R.A. Caruso, Chem. Mater. **13**, 109 (2001)
17. S.H. Joo, J.Y. Park, C.-K. Tsung, Y. Yamada, P. Yang, G.A. Somorjai, Nat. Mater. **8**, 126 (2009)
18. S. Laurent, S. Dutz, U.O. Häfeli, M. Mohmoudi, Adv. Colloid Interface Sci. **166**, 8 (2011)
19. J.-H. Lee, J.-T. Jang, J.-S. Choi, S.H. Moon, S.-H. Noh, J.-W. Kim, J.-G. Kim, I.-S. Kim, K.I. Park, J. Cheon, Nat. Nanotechnol. **6**, 418 (2011)
20. X.L. Liu, Y. Yang, C.T. Ng, L.Y. Zhao, Y. Zhang, B.H. Bay, H.M. Fan, J. Ding, Adv. Mater. **27**, 1939 (2015)
21. X.L. Liu, H.M. Fan, J.B. Yi, Y. Yang, E.S.G. Choo, J.M. Xue, D.D. Fan, J. Ding, J. Mater. Chem. **22**, 8235 (2012)
22. K. Hayashi, M. Nakamura, W. Sakamoto, T. Yogo, H. Miki, S. Ozaki, M. Abe, T. Matsumoto, K. Ishimura, Theranostics **3**, 366 (2013)
23. W. Rao, Z.-S. Deng, J. Liu, Crit. Rev. Biomed. Eng. **38**, 101 (2010)
24. S.S. Park, M.S. Moorthy, C.-S. Ha, NPG Asia Mater. **6**, e96 (2014). https://doi.org/10.1038/am.2014.13
25. M. Stubbs, P.M. McSheehy, J.R. Griffiths, C.L. Baseford, Mol. Med. Today **6**, 15 (2000)
26. A. Fu, R.J. Wilson, J. Mullenix, C. Earhart, D. Akin, S. Guccione, S.X. Wang, S.S. Gambhir, ACS Nano **6**, 6862 (2012)
27. J. Jiao, C. Liu, X. Li, J. Liu, D. Di, Y. Zhang, Q. Zhao, S. Wang, J. Colloid Interface Sci. **483**, 343 (2016)
28. Y. Zhu, Y. Fang, S. Kaskel, J. Phys. Chem. C **114**, 16382 (2010)
29. M.S. Moorthy, D.-J. Seo, H.-J. Song, S.S. Park, C.-S. Ha, J. Mater. Chem. A **1**, 12485 (2013)
30. I.I. Lungu, M. Radulescu, G.D. Mogosanu, A.M. Grumezescu, Rom. J. Morphol. Embryol. **57**, 23 (2016)
31. E. Ruiz-Hernández, A. López-Noriega, D. Arcos, I. Izquierdo-Barba, O. Terasaki, M. Vallet-Regí, Chem. Mater. **19**, 3455 (2007)
32. G. Rydzek, P. Schaaf, J.-C. Voegel, L. Jierry, F. Boulmedais, Soft. Mater. **8**, 9738 (2012)
33. M.S. Moorthy, J.-H. Bae, M.-J. Kim, S.-H. Kim, C.-S. Ha, Part. Part. Syst. Charact. **30**, 1044 (2013)
34. M.S. Moorthy, H.-J. Cho, E.-J. Yu, Y.-S. Jung, C.-S. Ha, Chem. Commun. **49**, 8758 (2013)
35. B.J. Kim, S. Kim, D.X. Oh, A. Masic, H.J. Cha, D.S. Hwang, J. Mater. Chem. B **3**, 112 (2015)
36. P. Sun, J. Wang, X. Yao, Y. Peng, X. Tu, P. Du, Z. Zheng, X. Wang, ACS Appl. Mater. Interfaces **6**, 12495 (2014)
37. K. Hayashi, M. Moriya, W. Sakamoto, T. Yogo, Chem. Mater. **21**, 1318 (2009)
38. K. Hayashi, K. Ono, H. Suzuki, M. Sawada, M. Moriya, W. Sakamoto, T. Yogo, ACS Appl. Mater. Interfaces **2**, 1903 (2010)
39. K. Hayashi, K. Ono, H. Suzuki, M. Sawada, M. Moriya, W. Sakamoto, T. Yogo, Chem. Mater. **22**, 3768 (2010)
40. R. Pieters, A.H. Loonen, D.R. Huismans, G.J. Broekema, M.,W. Dirven, M.W. Heyenbrok, K. Hahlen, A.J. Veerman, Blood, **76**, 2327 (1990)
41. M. Yu, J. Lin, J. Feng, Chem. Mater. **17**, 1783 (2005)
42. M.S. Moorthy, H.-J. Song, J.-H. Bae, S.-H. Kim, C.-S. Ha, RSC Adv. **4**, 43342 (2014)
43. H.-M. Song, J.I. Zink, Phys. Chem. Chem. Phys. **18**, 24460 (2016)
44. E. Ruiz-Hernández, A. López-Noriega, D. Arcos, I. Izquierdo-Borba, O. Terasaki, M. Vallet-Regí, Chem. Mater. **19**, 3455 (2007)
45. S. Gai, P. Yang, P. Ma, D. Wang, C. Li, X. Li, N. Niu, J. Lin, J. Mater. Chem. **21**, 16420 (2011)
46. C.P. Bean, J. Appl. Phys. **30**, 120 (1959)
47. K. Maier-Hauff, F. Ulrich, D. Nestler, H. Niehoff, P. Wust, B. Thiesen, H. Orawa, V. Budach, A. Jordan, J. Neurooncol. **103**, 317 (2011)
48. F.K. van Landeghem, K. Maier-Hauff, A. Jordan, K.T. Hoffmann, U. Gneveckow, R. Scholz, B. Thiesen, B. Bruck, A. von Deimling, Biomaterials **30**, 52 (2009)
49. K. Maier-Hauff, R. Rothe, R. Schlz, V. Gneveckow, P. Wust, B. Thiesen, A. Feussner, A. von Deimling, N. Waldoefner, R. Felix, A. Jordan, J. Neurooncol. **81**, 53 (2007)
50. P. Moros, S.K. Jones, B.N. Gray, Int. J. Hyperth. **18**, 267 (2002)
51. X.-Q. Zhang, M.-G. Zeng, S.-P. Li, X.-D. Li, Colloids Surf. B **117**, 98 (2014)
52. Y. Hu, Y. Ding, D. Ding, M.J. Sun, L.Y. Zhang, X.Q. Jiang, C.Z. Yang, Biomacromolecules **8**, 1069 (2007)